Building and Environment 215 (2022) 108971

Contents lists available at ScienceDirect

Building and Environment

journal homepage: www.elsevier.com/locate/buildenv

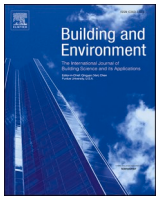

The use of machine learning to determine moisture recovery in a heat wheel and its impact on indoor moisture

Peng Liu [a,*], Maria Justo Alonso [a,b], Hans Martin Mathisen [b], Anneli Halfvardsson [c]

[a] SINTEF Community, Trondheim, Norway
[b] Department of Energy and Process Engineering, Norwegian University of Science and Technology, Trondheim, Norway
[c] Department of Research & Technology, Flexit AS, Ørje, Norway

ARTICLE INFO

Keywords:
Moisture recovery
Heat wheel
Indoor relative humidity
Condensation

ABSTRACT

Balanced mechanical ventilation equipped with heat recovery has been widely adopted in cold climates to ensure an acceptable indoor environment in energy-efficient buildings. An acknowledged trend to achieve more energy savings is to increase the temperature efficiency of heat recovery. As one of the efficient heat recovery technologies extensively used in Nordic countries, the rotary non-hygroscopic heat wheel yields high-temperature efficiency with low frosting risk. Due to the increasing temperature efficiency to comply with the tightened energy performance requirements, moisture recovery in heat wheels may occur more frequently and intensively. Moisture transfer from the extracted air to the supply air in non-hygroscopic heat wheels is not well known and scarcely studied. The impact of the resulting moisture recovery in heat wheels on indoor humidity is unclear.

This study uses machine learning algorithms to model and predict moisture recovery in a heat wheel. The effects of this moisture recovery on the supply and extract air, and indoor moisture levels in different rooms are analytically assessed for a selected single family house. The highest moisture recovery efficiency can reach 68%, and the yearly average value is 19% for the heat wheel in this study. For the specific studied single-family house, the heat wheel's moisture recovery introduces higher peaks in the supply air, bedrooms and living room. In general, the presence of moisture recovery in the heat wheel has a relatively limited effect on indoor humidity levels for a well-insulated and airtight house with the least amount of moisture generation scheme.

1. Introduction

High-insulation and airtightness levels are more strictly prescribed in cold climates to achieve energy-efficient buildings [1]. In these premises, highly efficient heat recovery ventilation systems have been recommended or required to reduce ventilation energy use. For instance, heat recovery with temperature efficiency higher than 80% in practice is usually needed to comply with Norwegian building regulation TEK 17 for residential buildings [1]. The increasingly tightened requirement on temperature efficiency for heat wheels in cold climates may lead to the more frequent occurrence and intensive amount of moisture recovery. The moisture transfer in heat wheels is, in turn, interrelated to indoor humidities that crucially influence indoor comfort, mould growth, building structure and occupants' health [2,3].

Intended and unintended moisture transfer in heat recoveries can occur with different mechanisms. Membrane plate exchangers, which enable both heat and moisture recovery, have attracted more attention recently for cold climates [4–7]. Membrane energy exchangers can mitigate frost formation in the heat exchanger and improve indoor "dry air" conditions by transferring humidity from extract air to supply air [8–10]. However, moisture recovery may delay the dilution of moisture peaks when the indoor air is already too humid. Rotary heat exchangers recover heat efficiently and have a lower frosting risk than plate heat exchangers. Thus, they have been extensively applied in Nordic countries. Rotary heat exchangers are divided into non-hygroscopic heat wheels and hygroscopic energy wheels based on the matrix surface's moisture sorption characteristics. Aluminium is usually used in non-hygroscopic heat wheel matrixes. In the non-hygroscopic heat wheel, the moisture transfer occurs through condensation in the extract air side and re-evaporation in the supply air side. When the extract air close to the wheel matrix surface is cooled down to the dew point, the condensation may form on the interior matrix surfaces, and it sequentially rotates and re-evaporate to the dry supply air. For the hygroscopic heat wheels, the moisture will be directly absorbed in the extract airside and desorbed to the supply air with the continuous wheel rotation, not

* Corresponding author.
E-mail address: peng.liu@sintef.no (P. Liu).

https://doi.org/10.1016/j.buildenv.2022.108971
Received 11 February 2022; Received in revised form 3 March 2022; Accepted 7 March 2022
Available online 17 March 2022

Nomenclature parameters

c_pSpecific heat capacity of aluminium [J/(kg•K)]i Specific heat capacity of aluminium [J/(kg•K)]tTime index
kThermal conductivity [W/(mK)]mMass flow rate of ventilation air [kg/s]N Thermal conductivity [W/(mK)]mMass flow rate of ventilation air [kg/s]NNumber of data
P_cCondensation potential [kg/kg]tTemperature [℃]
V Condensation potential [kg/kg]tTemperature [°C]
VRoom volume [m^3]

wHumidity ratio [kg/kg]Abbreviations

AHU	Air handling unit
GPR	Gaussian process regression
RH	Relative humidity
RMSE	Root mean square error
SVM	Support vector machine

Greek letters

η	EfficiencySubscript
amb	Ambient
ext	Extract
inf	Infiltration
out	Outdoor
sat	Saturated
sup	Supply
vent	Ventilation

2. Particles and dust may partially or fully foul the matrix surface. The accumulation of these fouling materials will also act as a hygroscopic coating on the heat transfer surface.

The moisture transfer mechanisms in heat wheels involves (1) condensation and re-evaporation that is the intended moisture transfer, (2) unintended moisture transfer due to oxidated or fouled surface and (3) intended and unintended moisture transfers, which may co-exist and be coupled in practice. The moisture transfer through condensation and re-evaporation for heat wheels, which is referred to intended moisture transfer in this study, has been investigated numerically and experimentally [23–25].The unintended moisture transfer in heat wheels, which is less known, is barely studied due to the unclear surface physics and the actual complexity and difficulty for modelling. To the authors' knowledge, there is no published study on modelling the moisture recovery in a heat wheel that considers both intended and unintended moisture transfer.

A schematic of a heat wheel matrix with an oxidated or fouled surface and condensation water is shown in Fig. 1. The moisture transfer resulting from condensation and the hygroscopicity of the aged surface may take place independently or simultaneously depending on the operating conditions and matrix surface characteristics.

Indoor air humidity is imperative for the indoor environment and building materials. "Dry indoor air" is a major complaint from occupants in residential and office buildings during winter in cold climates [2,26]. The common low humidity disturbance is sensory irritation in the eyes and upper airways [2,27]. Increasing indoor air humidity may ease these symptoms. On the other hand, if the relative humidity (RH) is too high, "too humid air" may cause mould growth and building material damage [28,29]. A widely acceptable and desired RH range has been a

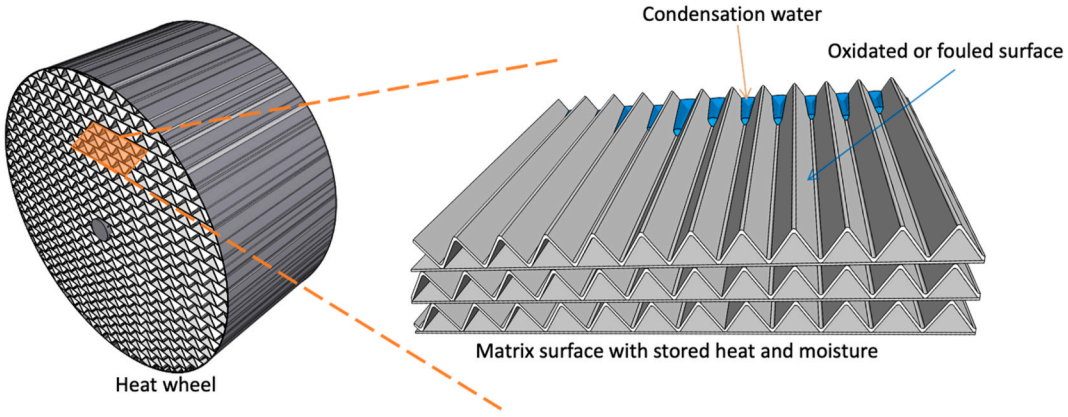

Fig. 1. Schematic view of a heat wheel and oxidated or fouled matrix surface with condensation.

necessarily through the condensation and re-evaporation processes. The application of non-hygroscopic and hygroscopic wheels have been numerically and experimentally investigated in recent years [10–20]. However, the effects of moisture transfer from heat recovery especially for non-hygroscopic heat wheel on indoor humidity are under-explored. The authors have not found substantial work referring to this topic.

In a heat wheel with a non-hygroscopic surface, the moisture transfer is usually only expected when condensation or frosting occurs. In practice, the non-hygroscopic aluminium surface may, however, perform with hygroscopic-like features due to changes to the surface characteristics during the lifetime of heat wheels. Twofold phenomena may cause the unintended changes in surface characteristics and the resulting moisture transfer in heat wheels [22]:

1. The untreated aluminium surface in the heat wheel matrix is active to react with oxygen from the air. The oxidated aluminium surface will perform hygroscopically.

long-standing dispute. The Norwegian Institute of Public Health suggests that for indoor climates "too high humidity" refers to RH above 70% and "extremely low humidity" RH below 20% [30]. The use of humidifiers is not recommended, as they risk polluting of the indoor climate [30]. Moisture recovery is recognised as one of the operative manners to improve the dry conditions [31]. The indoor moisture loads and moisture generation schedules have been investigated in numerous research [3,32–36]. Nevertheless, the effects of moisture recovery on indoor RH have not been adequately studied for highly insulated and airtight buildings in cold climates. Smith and Svendsen [3] developed moisture balance equations focusing on single-room ventilation equipped with a non-hygroscopic heat wheel in a temperate climate (Denmark). The results are compared with whole dwelling ventilation systems. They concluded that the rotary heat wheel recovers excessive moisture from kitchens and bathrooms. This leads to mould growth risk in tempered climates in the specified context of their study.

In the current study, supervised machine learning algorithms are

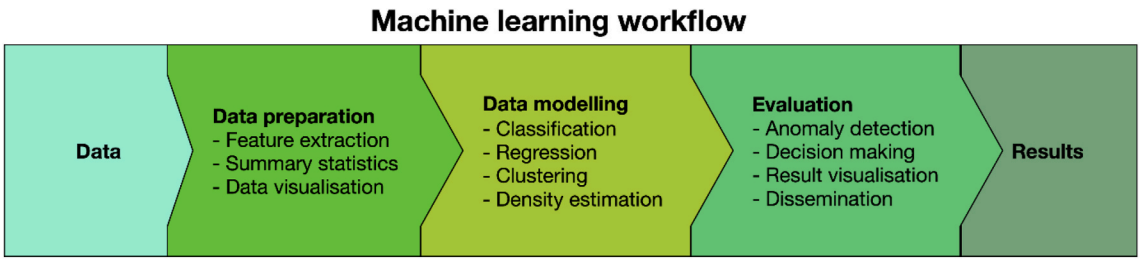

Fig. 2. A workflow of machine learning modelling.

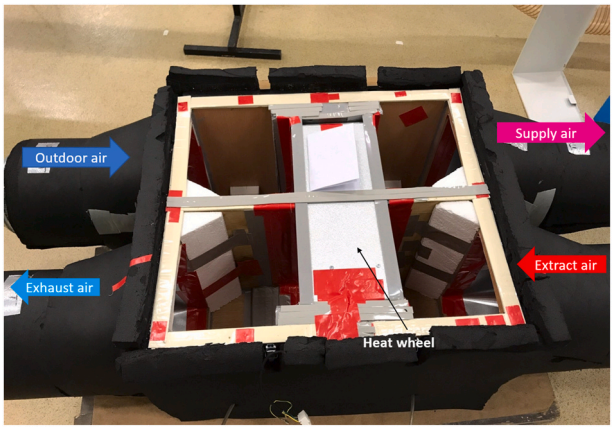

Fig. 3. Test unit for the heat wheel complying with testing standard EN 308.

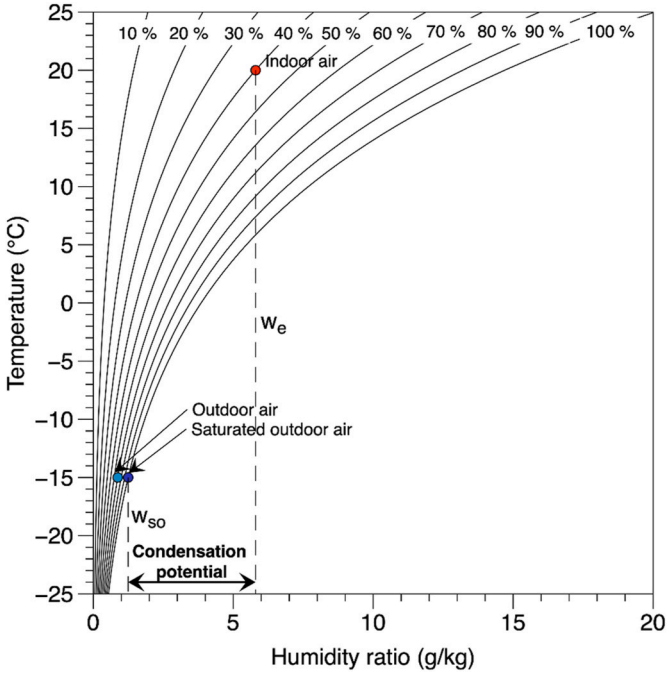

Fig. 4. Condensation potential in a Mollier chart.

employed to model moisture recovery in a heat wheel using experimental data as the model training database. The best-trained model predicts moisture recovery for the heat wheel. Our main contributions in this paper are as follows:

1. This study models moisture recovery in a heat wheel using machine learning algorithms. The moisture recovery model is able to take into account all possible causality leading to moisture transfer for the heat wheel. It not only accounts for moisture transfer from condensation and re-evaporation but also includes the effects of surface hygroscopicity changes such as oxidated and/or the fouled heat transfer matrix surface.
2. The developed machine learning model considers all the physical parameters affecting moisture recovery in the measured case, not only the mass transfer due to condensation. Thus, the prediction is more accurate.
3. The moisture recovery predictions are coupled with an in-house moisture generation and ventilation simulation tool through moisture balance equations. Yearly moisture recovery efficiencies with a 95% confidence interval and indoor RH for different rooms in a high (2-min) time resolution are revealed for a single-family house in Oslo, Norway.
4. The effects of the moisture recovery in the heat wheel on the RH of supply and extract air, and RH of different rooms (refer to Fig. 6), are assessed by comparing the scenario with and without adding moisture recovery for a single-family house.

With these highlighted contributions, the paper attempts to using machine learning to investigate the moisture transfer in heat wheel considering condensation and matrix surface changes In addition, the effect of the moisture recovery on indoor humidity is assessed with moisture balance in ventilation.

The structure of this paper is as follows: the machine learning model, moisture generation, ventilation setup and moisture balance equations are presented in Section 2 (Methods). Section 3 (Results and Discussion) assesses and tests the trained model. The predicted moisture efficiency for one year and indoor RH for different rooms, including and excluding the effects of moisture recovery, are presented in section 3. Weekly RH plots of week 2 and week 18 are selected to illustrate the results in the winter season and transition season.

2. Methods

In this section, the machine learning model of moisture transfer in a heat wheel and the indoor moisture and ventilation simulation model are presented.

2.1. Machine learning models for the moisture recovery of the heat wheel

Fig. 2 illustrates a generic workflow of the machine learning method. Section 2 (Methods) and section 3 (Results) briefly present the implementation of each step for this study by following this workflow. Measurements of moisture and heat transfer in a heat wheel under different operating conditions are used to train machine learning models. This study tests different machine learning models to learn from the data set. The best model is defined as the one with the minimum root mean square error (RMSE).

2.1.1. Dataset and data preparation

The measured parameters include the temperature and relative humidity at the inlets and outlets of the heat wheel, as well as the airflow

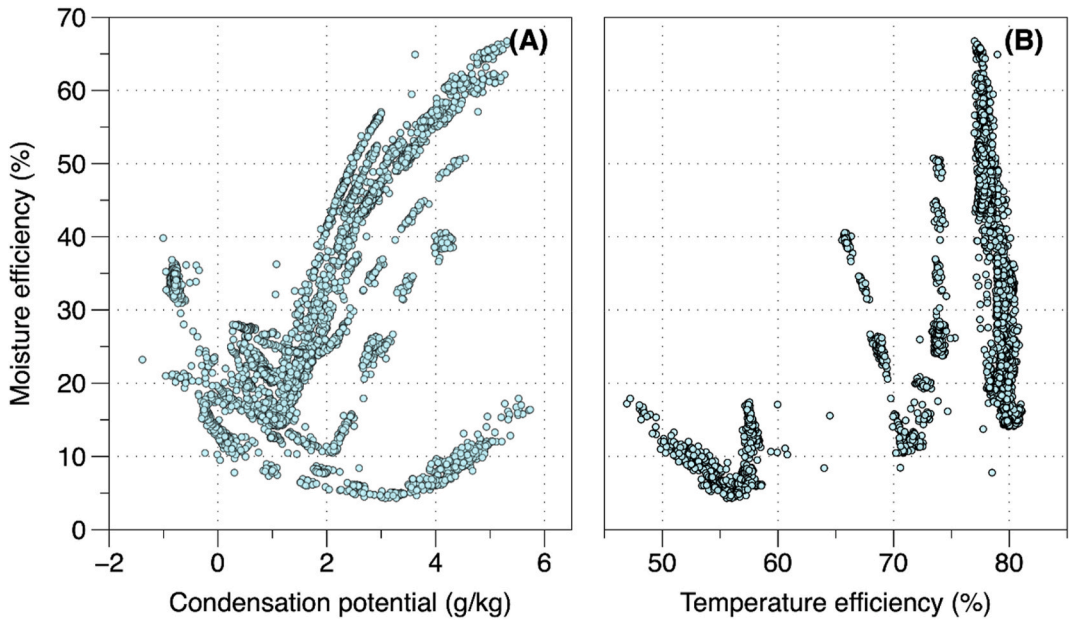

Fig. 5. Measurement data visualisation (A) Moisture efficiency vs condensation potential (B) Moisture efficiency vs temperature efficiency.

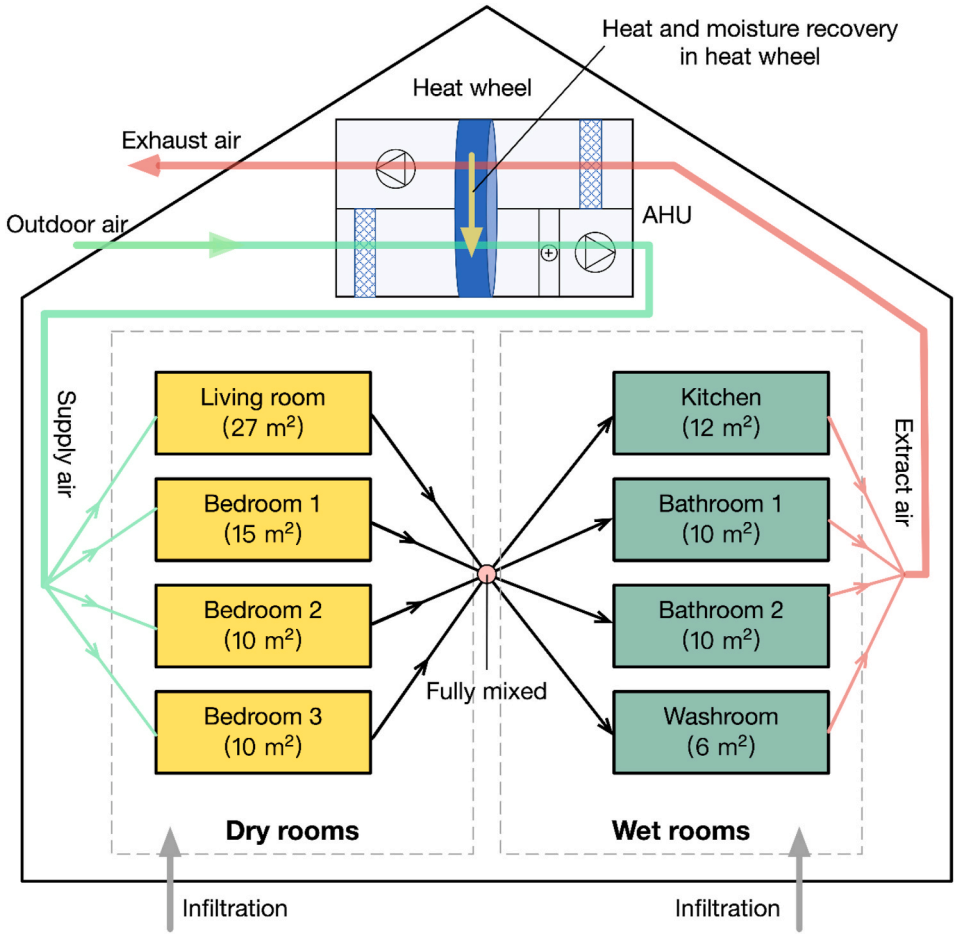

Fig. 6. The studied building and ventilation air movement.

rate and pressure drop for each side and wheel's rotational speeds. Temperature and moisture efficiency are calculated with the measured parameters provided in equations (1)–(3). The experimental measurements were performed using a testing unit as shown in Fig. 3, complying with the heat recovery testing standard EN308 [37]. The measurement data, which contains 4736 observations for each measured parameter, are aggregated and used for the model training. One hundred measurement data points extracted randomly from the database are kept

Table 1
Heat wheel parameters and testing conditions.

Heat wheel parameters	Value	Testing conditions	Range
Wheel depth	150 mm	Ventilation rate	100 m^3/h – 250 m^3/h
Wheel diameter	400 mm	Rotary speed	1 RPM – 8 RPM
Wall thickness	0.055 mm	Warm (indoor) air RH	20%–52%
Wall material	Aluminium $k = 205$ W/(m•K) $c_p = 900$ J/(kg•K)	Cold (outdoor) air temperature	$-15\,^{\circ}C - 5\,^{\circ}C$
Corrugation shape	Sinusoidal Channel height: 1.5 mm Channel period: 3.0 mm		

Table 2
Machine learning models used for training data in this study and RMSE.

ID	Learning models	RMSE	Algorithm
1	Linear regression	0.1018	Linear regression
2	Interactions linear regression	0.0982	
3	Robust linear regression	0.1019	
4	Stepwise linear regression	0.0982	
5	Fine tree	0.0221	Tree
6	Medium tree	0.0226	
7	Coarse tree	0.0268	
8	Linear Support Vector Machine (SVM)	0.1109	SVM
9	Quadratic SVM	0.0683	
10	Cubic SVM	0.1436	
11	Fine Gaussian SVM	0.0224	
12	Medium Gaussian SVM	0.0291	
13	Coarse Gaussian SVM	0.0588	
14	Boosted trees ensemble	0.0292	Ensemble
15	Bagged trees ensemble	0.0205	
16	Squared exponential Gaussian process regression (GPR)	0.0205	GPR
17	Matern 5/2 GPR	0.0196	
18	**Exponential GPR**	**0.0188**	
19	Rational quadratic GPR	0.0190	

Table 3
The best-case scenario of indoor moisture release for different activities.

Sources	Room	Frequency	Units	Production
Cooking method	Kitchen	–	–	Electric
Cooking load	Kitchen	–	kg per day per household	0.2 (Breakfast) 0.3 (Lunch) 0.7 (Dinner)
Dishwasher load	Kitchen	Daily	kg/day	0.05
Cleaning	All	Weekly	kg/m^2	0.005
			kg/day	0.04
Shower load	Bathroom	3 showers/day	kg/shower	0.20
			kg/day	0.6
Plants	Living room	–	kg/day	0.06
Awake adult moisture release	Living room/ Kitchen	–	kg/hour/person	0.03
Sleeping	Bedroom	Daily	kg/hour/person	0.02

outside the training data and used as the model verification dataset.

The tested heat wheel is designed for a single-family house heat recovery ventilation. The nominal temperature efficiency is 80.9% at a ventilation rate of 208 m^3/h. The testing conditions and geometry parameters of the heat wheel are summarised in Table 1.

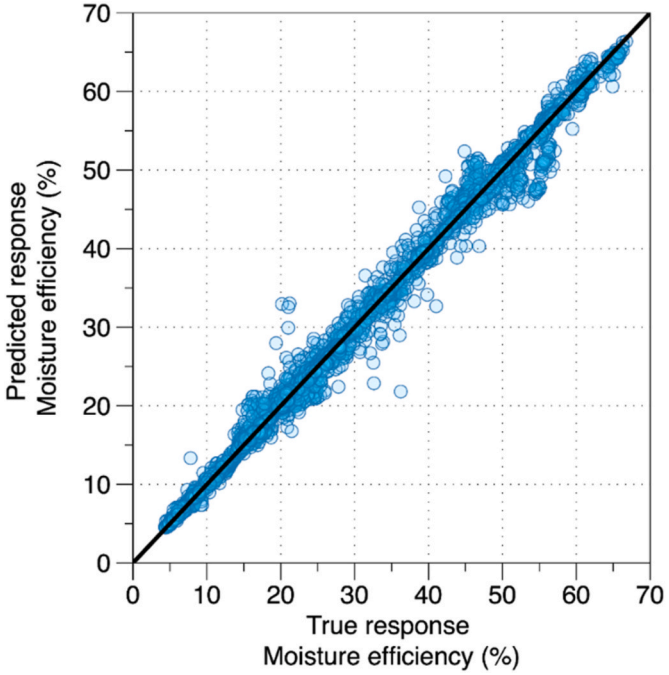

Fig. 7. The predicted response vs true response.

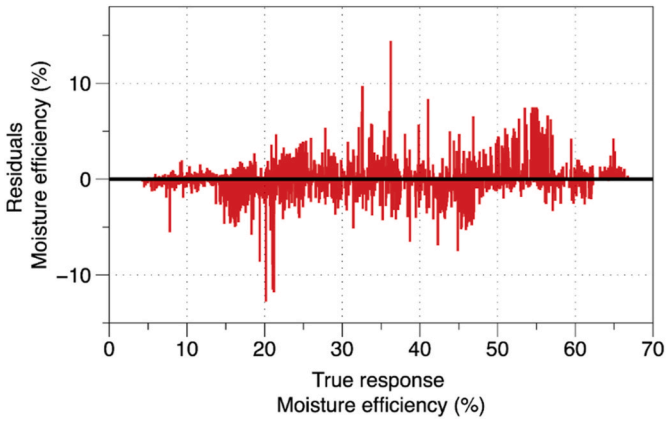

Fig. 8. Model residuals vs true response.

The moisture efficiency for balanced airflow rates, as in this case, is given by

$$\eta_m = \frac{w_{sup} - w_{out}}{w_{eA} - w_{out}} \tag{1}$$

The temperature efficiency for balanced heat capacities is

$$\eta_t = \frac{t_{sup} - t_{out}}{t_{ext} - t_{out}} \tag{2}$$

The condensation potential is a humidity ratio difference between indoor warm air and saturated outdoor cold air defined by Eq. (3). The condensation potential indicates the maximum amount of moisture transfer per unit of airflow rate from the exhaust to the supply airside.

$$P_c = w_{ext} - w_{sat,out} \tag{3}$$

An example of condensation potential in a Mollier chart is given in Fig. 4.

Besides condensation potential, the high temperature efficiency of a heat wheel may intensify the moisture transfer as the condensation

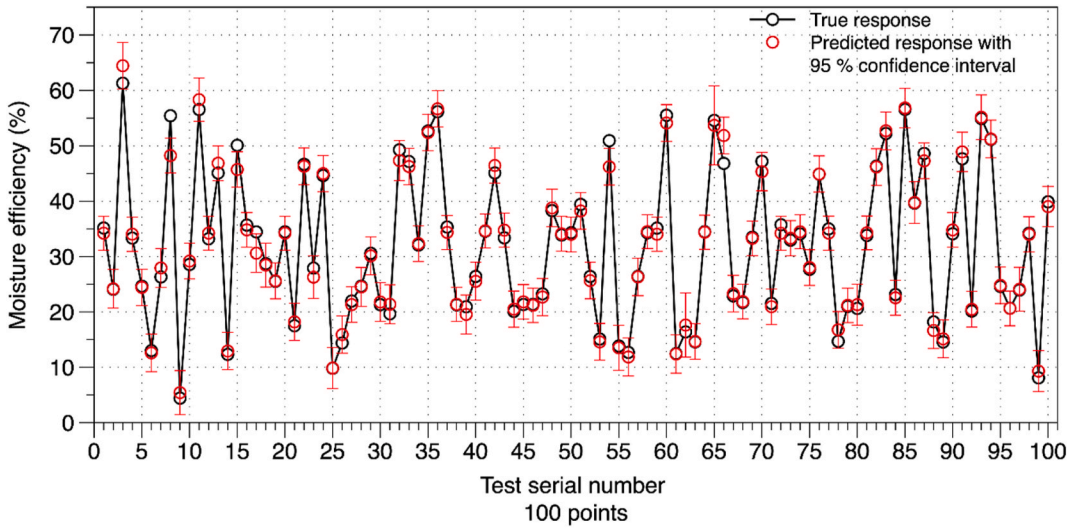

Fig. 9. Model prediction test with 100 data points.

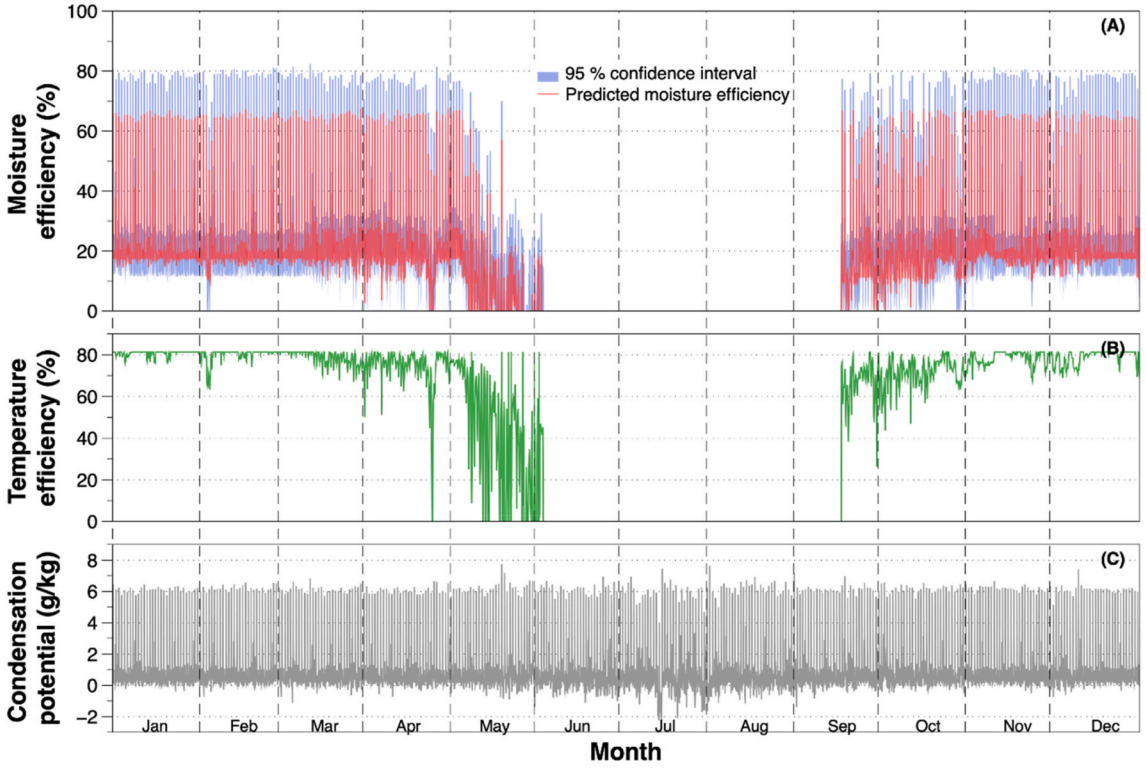

Fig. 10. Annual moisture efficiency prediction with a 95% confidence interval using the GPR model.

occurs more frequently on these surfaces with higher heat exchange rates. The training database (measured data) is visualised in Fig. 4. It can be seen that the moisture efficiency spreads widely against condensation potential and temperature efficiency. Moisture transfer cannot be well accounted for by mere condensation potential. The condensation potential and temperature efficiency are computed and used as the predictors determining moisture recovery for heat wheels. The calculated moisture transfer efficiency from measured humidities at inlets and outlets is treated as the true response in this supervised learning. The moisture transfer in a heat wheel occurs when the air temperature at matrix surface is below the dew point due to condensation. The non-zero moisture efficiency for negative condensation potentials indicates that moisture transfer occurs even when no condensation appears in the heat wheel, as shown in Fig. 5 A. The authors hypothesise that these values, which are not associated with condensation, may infer another effect affecting the moisture recovery. As the heat wheel is not new (the wheel was manufactured in 2016 and the test was carried out in 2018), the hypothesis of having an oxidation or fouling layer acting as hygroscopic material gains weight. However, this cannot be proven with the existing data. The non-hygroscopic heat wheel with oxidation or a fouling layer performs as a hygroscopic sorption wheel. The similar trends have been observed for the hygroscopic wheels with moisture recovery due to moisture transfer through both desiccant material and condensation [38]. Whatever the reason behind this effect, machine learning learns from the measurements and can predict the increased moisture recovery on this heat wheel. The sorption characteristic cannot be determined

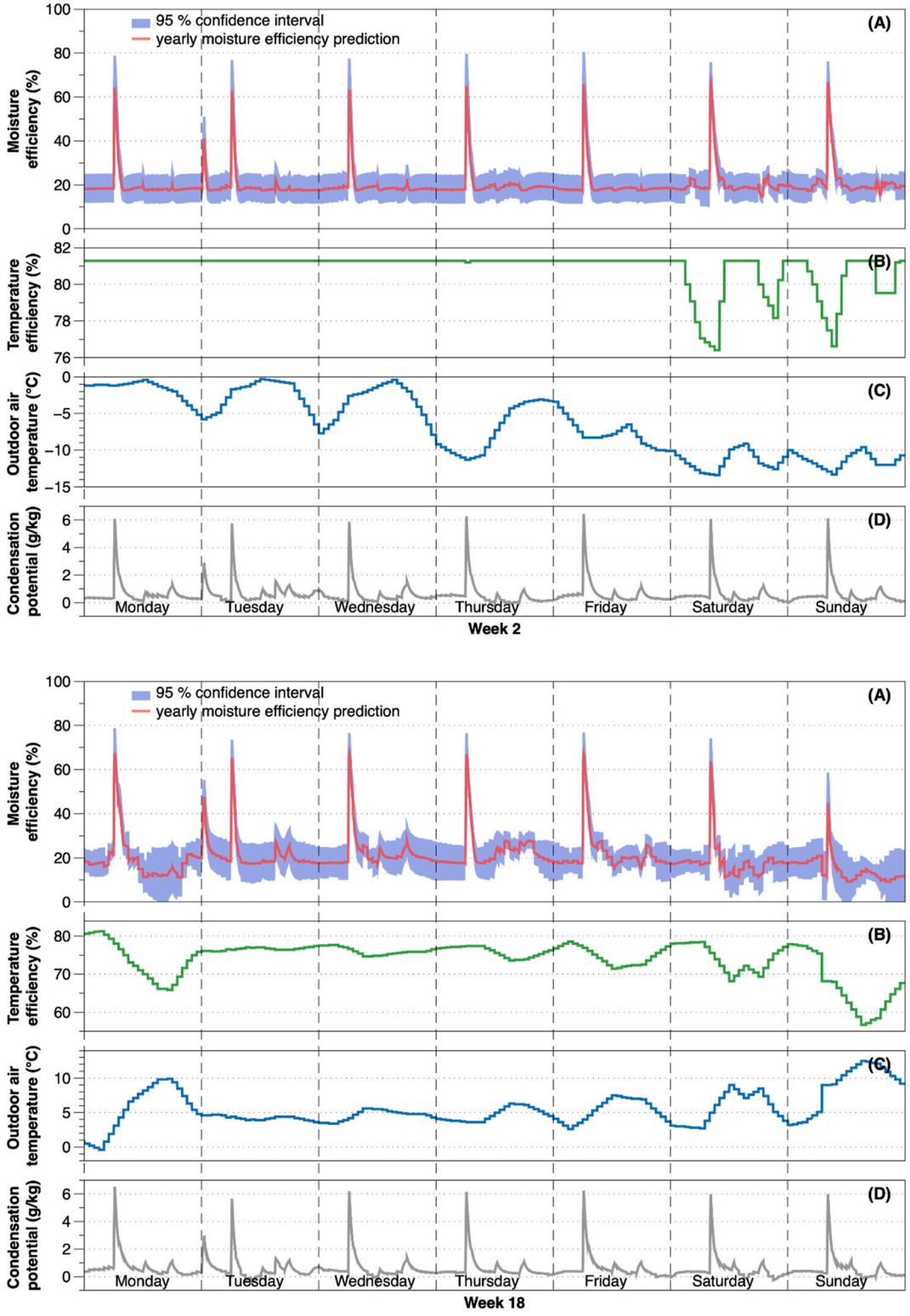

Fig. 11. Week 2 and week 18 plots for (A) moisture efficiency, (B) temperature efficiency, (C) outdoor air temperature and (D) condensation potential.

quantitively with the existing measures. Further studies using other heat wheels are needed to extend these conclusions to other wheels.

2.1.2. *Moisture recovery modelling using machine learning*

This study uses nineteen different machine learning models built into the Regression Learning Toolbox in MATLAB. The models can be categorised into five supervised learning algorithms, as shown in Table 2. The study activated 5-fold cross-validation to prevent model overfitting. The Root Mean Square Error (RMSE), defined in Equation (4), is used to evaluate the fitted models' accuracy.

$$RMSE = \sqrt{\frac{\sum_{i=1}^{N} (Predicted_i - Actural_i)^2}{N}} \tag{4}$$

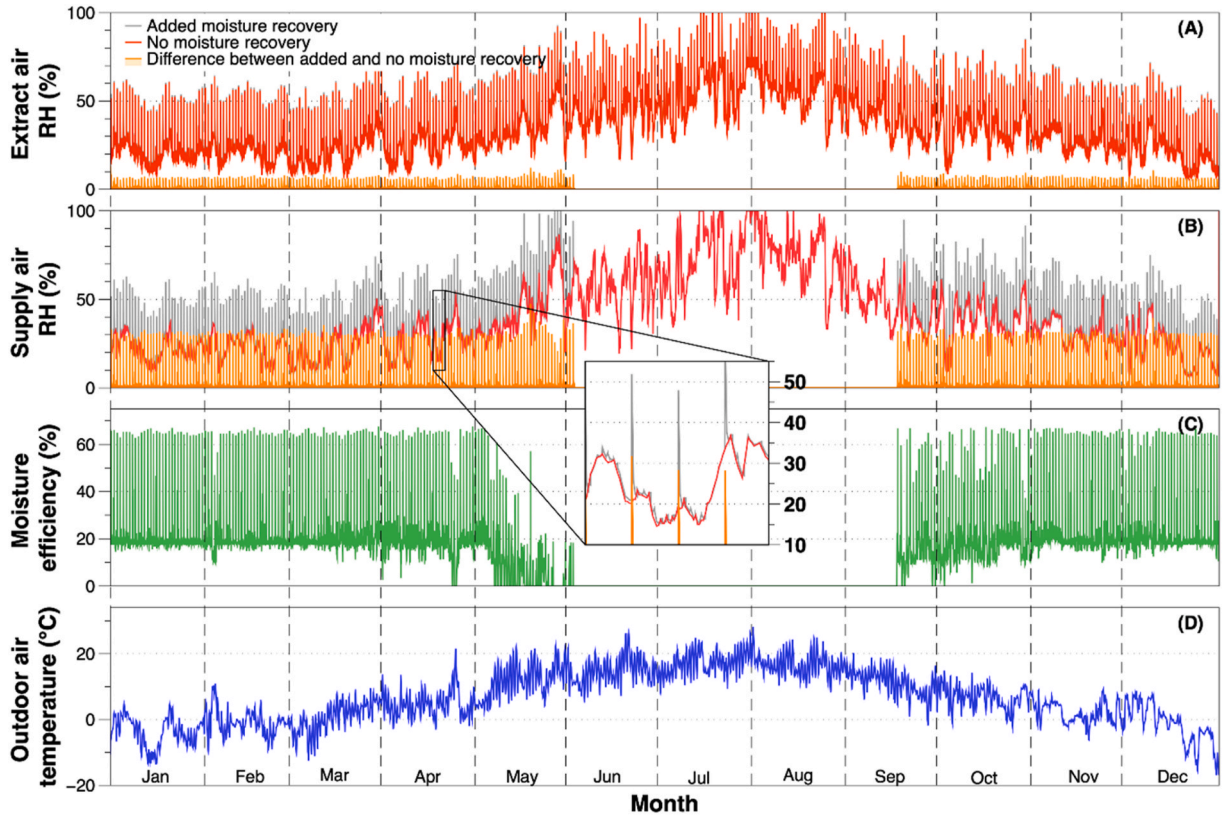

Fig. 12. Annual RH of extract and supply air including and excluding moisture recovery in the heat wheel.

RMSE measures how well the predicted data using one model fits the real (measured) data points. The RMSE results for the tested models are given in Table 2. The Exponential Gaussian Process Regression (GPR) model presents the minimum RMSE. Thus, the Exponential GPR is selected as the best learning algorithm and will be further used in this study to predict yearly moisture efficiency. GPR is a non-parametric Bayesian approach to regression problems. "A Gaussian process is a collection of random variables, any finite number of which have a joint Gaussian distribution." [39] A Gaussian process is implemented by the mean function and covariance function. The mean function $m(x)$ and covariance function $k(x,x')$ of a real process are defined as [39],

$$m(x) = \mathbb{E}[f(x)] \tag{5}$$

$$k(x,x') = \mathbb{E}[(f(x) - m(x))(f(x') - m(x'))] \tag{6}$$

The mean function gives the expected value at input x. The covariance function yields the association between the function values at different inputs x and x'. GPR is able to define the predictive distribution for the predicted results, which means a confidence interval can be obtained together with the predicted values.

2.2. Indoor moisture and ventilation system for a single-family house

The developed machine learning model of the tested heat wheel is coupled with a single-family house's ventilation and moisture production model. The combined models are used to investigate the influence of the heat wheel's moisture transfer on the indoor moisture levels. This section describes the building and the moisture generation and ventilation setup used to simulate a single-family house located in Oslo.

2.2.1. Building description

The modelled 100 m^2 single-family house has a volume of 240 m^3. The building envelope and airtightness complies with the Norwegian building regulation TEK 17 [1]. The house has eight rooms, split into wet rooms - two bathrooms, one laundry room and one kitchen - and dry rooms - three bedrooms and one living room. The floor areas of these different rooms are given in Fig. 6. Two adults and one child spend 13 h per day indoors. A schematic view of the air loop and the air handling unit is shown in Fig. 5.

2.2.2. Ventilation

The ventilation rate is always 208 m^3/h supplied to the dry rooms flowing in cascade to the wet rooms where it is extracted. The air from the dry rooms is fully mixed before entering wet rooms, as indicated in Fig. 6. The supply air temperature is 18 °C. The room temperature for all rooms is 21 °C except for the bathroom, where the air temperature is 23 °C. The air handling unit is equipped with a rotary heat exchanger, with a temperature efficiency of 81.2% at a ventilation rate of 208 m^3/h. The heat wheel's temperature efficiency is controlled, adjusting the rotational speed to avoid the supply air temperature exceeding 18 °C and exhaust air temperature lower than −5 °C for frost protection. The heat recovery is stopped during summer (from June 1st to September 15th) to prevent overheating the supply air.

2.2.3. Moisture generation and moisture balance

The moisture generation schemes and simulation background for the whole-dwelling ventilation are derived based on [3,40]. The updated model is connected to the developed moisture recovery machine learning algorithm. The initial relative humidity in all rooms at the beginning of the simulation is 50%. The indoor moisture buffering effect from building materials and furniture is not considered in the model.

Equation (7) shows the moisture balance equation to calculate the indoor moisture. The balance is done every 2 min to capture rapid fluctuations of indoor humidity related to the activities.

$$m\frac{dw}{dt} = G_{sources}(t) + G_{in}(t) - G_{out}(t) \tag{7}$$

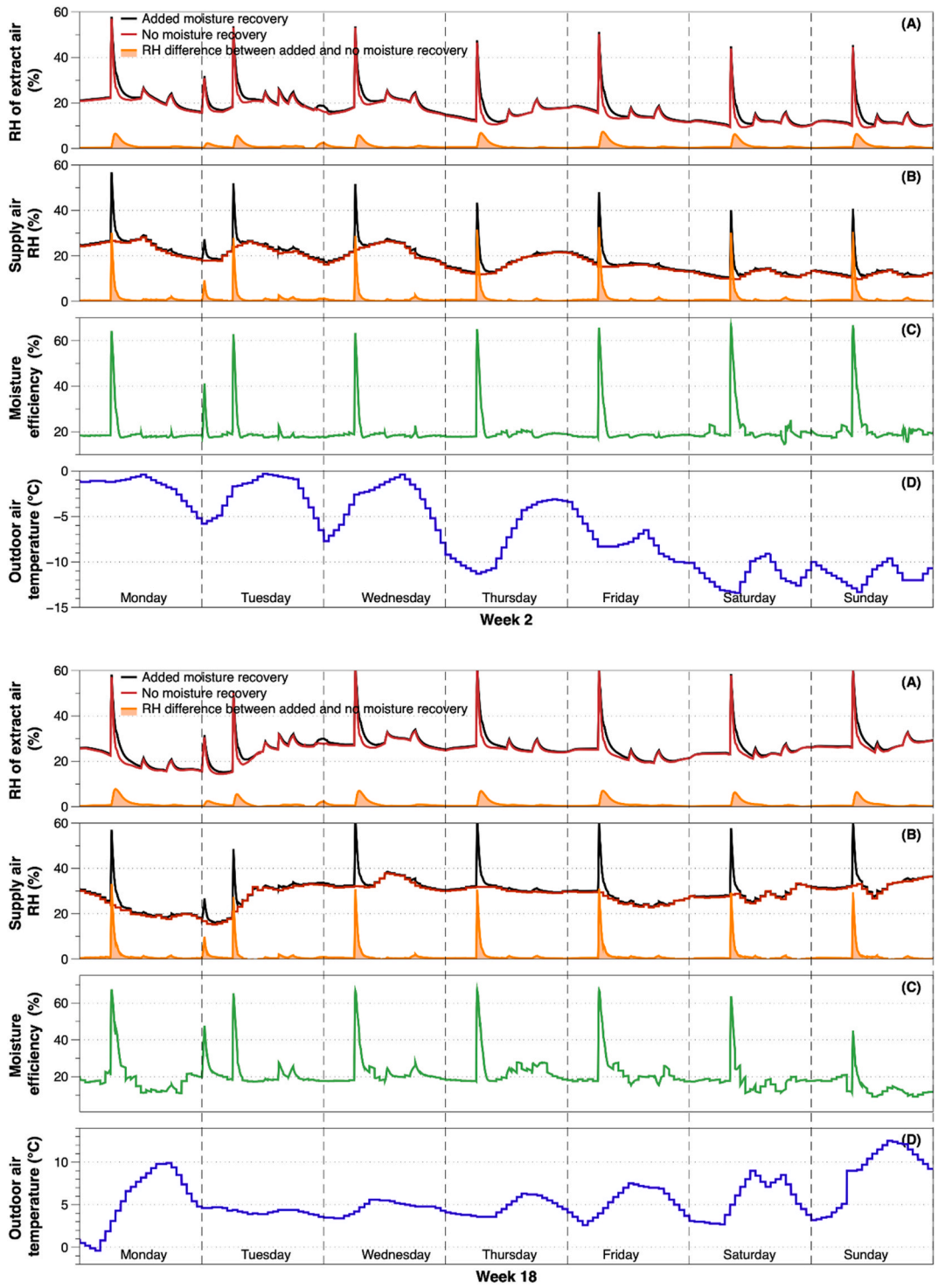

Fig. 13. Week 2 and week 18 plots for (A) extract air RH, (B) supply air RH, (C) moisture efficiency and (D) outdoor air temperature.

Table 4
Per cent of time duration for the reference year in different rooms.

Rooms	RH < 20%		RH 20%–60%		RH > 60%	
	Added moisture recovery	No moisture recovery	Added moisture recovery	No moisture recovery	Added moisture recovery	No moisture recovery
Kitchen	14.5%	16.4%	72.7%	71.1%	12.8%	12.5%
Bathroom	25.0%	27.6%	68.0%	65.7%	7.0%	6.7%
Living room	17.5%	20.2%	74.6%	72.1%	7.9%	7.7%
Bedroom	20.4%	23.1%	72.4%	69.8%	7.2%	7.1%

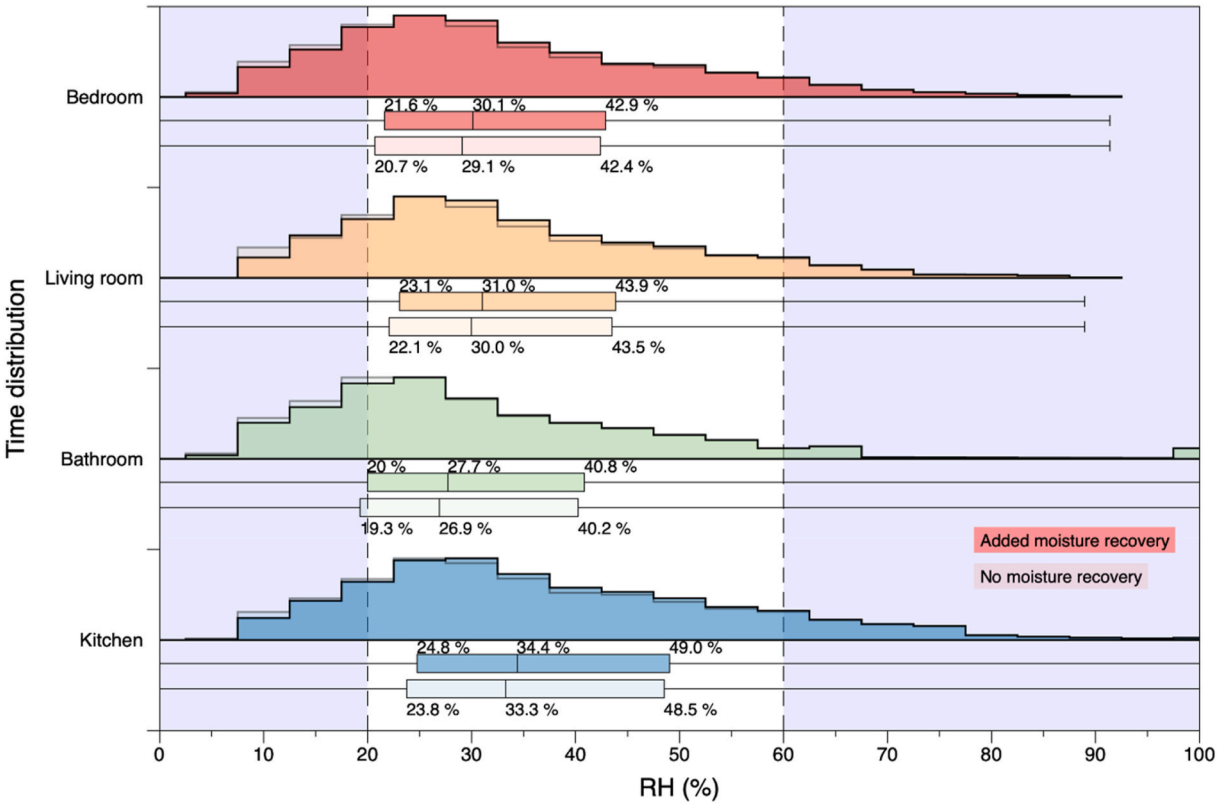

Fig. 14. Distribution of RH values for different rooms including and excluding moisture recovery.

For dry rooms, the study uses the following iteration to compute the room air's humidity ratio.

$$w_{dry,\ \ room,i+1} = w_{dry,\ room,i} + \frac{G_{room,i}}{(\rho V)_{room}} - N_{inf,room}\left[min\left(w_{sat,room}, w_{room,i}\right) - w_{amb,i}\right] - N_{vent,room}\left[min\left(w_{sat,room}, w_{room,i}\right) - w_{sup,room,i}\right] \quad (8)$$

The moisture ratio in the supply air $w_{sup,room,i}$ is the minimum of the sum of the outdoor air moisture ratio and the recovered moisture in the heat wheel or the saturated supply humidity ratio.

$$w_{sup,room,i} = min\left\{\left[w_{amb,i} + \eta_{m,i}\left(w_{ext,i} - w_{amb,i}\right)\right],\ w_{sup,sat}\right\} \quad (9)$$

$w_{ext,i}$, the moisture ratio of the air in the extract duct and the mixture of the extract air from the wet rooms, is calculated by Eq. (10).

$$w_{ext,i} = \frac{\sum\left(V_{wet,room} w_{wet,\ \ room,i}\right)}{\sum V_{wet,room}} \quad (10)$$

The moisture efficiency $\eta_{m,i}$ is the one predicted by the machine learning model developed in section 2.1.

The mixed air leaving all the dry rooms is supplied to the wet rooms. The moisture ratio of the mixed air from dry rooms is calculated from Eq. (11).

$$w_{dry,mixed,i} = \frac{\sum\left(V_{dry,room} w_{dry,\ \ room,i}\right)}{\sum V_{dry,room}} \quad (11)$$

In the wet rooms, the moisture ratio is determined similarly to in the dry rooms.

$$w_{wet,\ \ room,i+1} = w_{wet,\ room,i} + \frac{G_{room,i}}{(\rho V)_{room}} - N_{inf,room}\left[min\left(w_{sat,room}, w_{room,i}\right) - w_{amb,i}\right] - N_{vent,room}\left[min\left(w_{sat,room}, w_{room,i}\right) - w_{dry,mixed,i}\right] \quad (12)$$

Oslo's hourly weather data reference year, including outdoor air temperature, relative humidity, and wind speed, is duplicated to 2-min data and applied in the simulation. The moisture sources simulated are the lowest found in the literature for humans, animals, cooking, dish-washing, cleaning, showering, washing and drying clothes. The selected significant moisture sources are presented in Table 3.

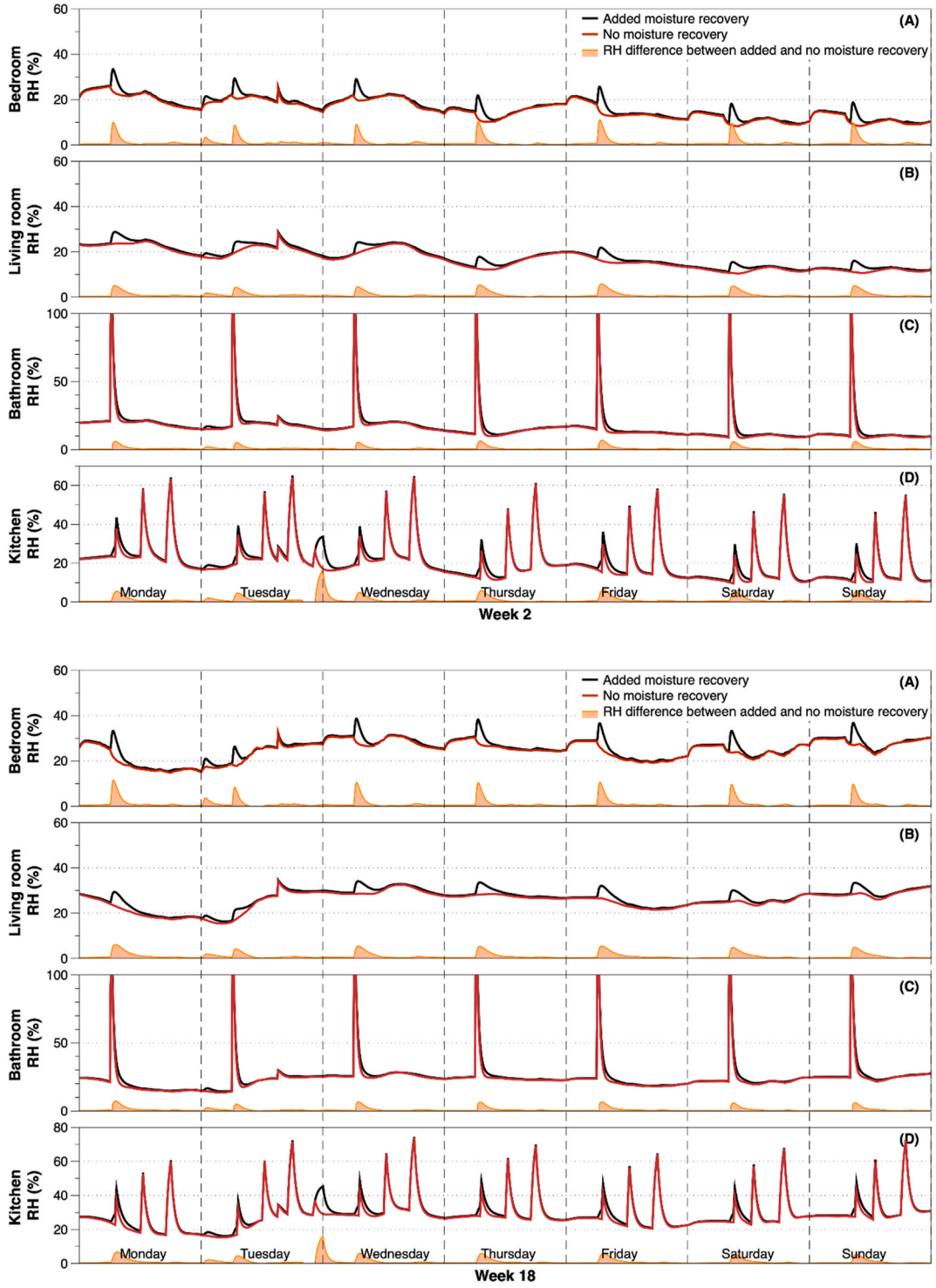

Fig. 15. Week 2 and week 18 plots of RH in (A) bedroom, (B) living room, (C) bathroom, and (D) kitchen.

3. Results and discussion

3.1. Model training

As explained in the method section, the temperature efficiency and condensation potential are extracted as features. The moisture efficiency is derived from the measured temperature and relative humidity at the heat wheel's inlet and outlet. The exponential Gaussian Process Regression, which has a minimum RMSE value, is selected as the best machine learning model in this study. The exponential GPR model's predicted response is plotted against the true response in Fig. 7.

The residuals plot in Fig. 8 indicates a good performance of the machine learning model. It can be seen from Fig. 8 that the residuals are scattered roughly symmetrically around zero and have no clear patterns in the residuals.

3.2. Validation of the machine learning model

The hundred data points randomly extracted and unseen by the model are used to validate the trained model's performance. The

moisture efficiency predictions with a 95% confidence interval are compared to the actual true response in Fig. 9. The model is capable of predicting the moisture efficiency for the randomly selected 100 test data points.

3.3. Moisture recovery efficiency in the heat wheel

The developed GPR machine learning model predicts the heat wheel's moisture transfer efficiency with two input parameters: temperature efficiency and condensation potential. Fig. 10 (A) shows annual moisture efficiency predictions and the 95% confidence interval. Fig. 10 (B) and (C) display the temperature efficiency and condensation potential, which are used as new input parameters for the GPR model to predict the moisture efficiency. The annual predicted average moisture efficiency is 19.2% when the heat wheel operates, and the maximum efficiency is 67.6%. Relatively high moisture efficiency (greater than 60%) appears when high condensation potentials exist, mainly due to showering. During most of the heat wheel operating time, the moisture efficiency is about 20% even when the condensation potential is zero or negative. As stated before, it is speculated that the non-hygroscopic heat wheel acts as a sorption wheel due to the unintended surface characteristic change possibly caused by surface oxidation or fouling. The temperature efficiency fluctuates significantly during spring and autumn as this is regulated to maintain supply air temperature at 18 °C. The moisture efficiency drops when the corresponding temperature efficiency is reduced.

Weekly plots of week 2 and week 18 for moisture and temperature efficiency, outdoor air temperature and condensation potential are presented to show more evident moisture efficiency variations. Fig. 11 shows week 2 (early in January) and week 18 (early in May) as examples of the weekly plots for winter season and spring season, respectively. Most of the peaks of moisture efficiency correspond to showering time when maximum condensation potentials appear. The peak at midnight on Tuesday is related to the operation of the dishwasher. The moisture efficiency for the rest of the time is relatively constant at 20% for week 2. During the weekend of week 2, the temperature efficiency is lowered for frost protection when the outdoor air temperature is extremely low. In week 18, the heat wheel's temperature efficiency is, however, reduced to prevent overheating the supply air.

The moisture recovery in the heat wheel adds moisture to the supply air affecting indoor moisture levels. Fig. 12 shows, for a whole year, the RH in extract air and supply air, including and neglecting the moisture recovery. The average difference of RH for extract air, including and excluding moisture recovery, as represented by the yellow line in Fig. 12 (A), is 1.1%, and the maximum difference is 13.4% during showering time. The corresponding difference for the supply air is respectively 1.4% and 47.5%, shown in Fig. 12 (B). The supply air RH, including moisture recovery, has high moisture recovery peaks corresponding to showering and cooking, as demonstrated by the magnification view in Fig. 12 (B).

The extract and supply air RH, including and excluding moisture transfer, outdoor air temperature and condensation potential for weeks 2 and 18 are plotted in Fig. 13. The influence of the moisture recovery on RH peaks in extract air is relatively low compared to the effect on supply air due to the air distribution, mixing and movement from dry to wet rooms for both week 2 and week 18. For week 2, RH in supply and extract air is lower than 20% for a large fraction of time. During week 18 it is generally over 20%. The drier supply air may cause this low indoor RH.

Table 4 shows the percentage of hours per year when the indoor air RH is below 20% and over 60%, both including and excluding moisture recovery. Over 65% of the time per year, indoor RH is in a range of 20%–60%. All the rooms in Table 4 experience extremely low indoor RH for more hours than they do too high RH. The overall time duration of "dry indoor air" accounts for around 20% of the year, which is about half of the wintertime. The moisture recovery in the heat wheel reduces the too low RH time by 2% on average. Its effects on too high RH time is less than 0.5%.

Fig. 14 shows the time duration, minimum, first quartile, median, third quartile and maximum of RH in different rooms for the scenarios both considering and not considering moisture recovery. For the selected four rooms, the indoor RH median during the reference year is around 30%. The time distribution of different RH both including and excluding moisture recovery is of similarity. It means the moisture recovery in the heat wheel has limited impacts on improving the dry room conditions in this case. The large area per person, high ventilation rates and dry outdoor air during winter in Oslo contribute to the low indoor RH, even if the effect of the moisture recovery is considered. Thus, we can conclude from Table 4 and Fig. 14 that the moisture recovery has relatively little effect on the RH for the studied heat wheel in this work.

Fig. 15 shows the weekly RH in different rooms for weeks 2 and 18. It can be found that higher peaks of RH for the dry rooms (bedroom and living room) appear during showering in which more indoor moisture is recovered to the supply air. The RH profiles in the wet rooms (bathroom and kitchen) are almost identical. All the rooms have dry indoor air (RH $<$ 20%) most of the time in week 2.

4. Conclusions

In this work, a model for heat recovery is obtained from machine learning analysis of measurements. Based on 4736 observations, this study is validated by predicting the moisture recovery in 100 unseen cases. The best GPR model predicts annual moisture efficiency with a 95% confidence interval for the heat wheel. Moisture recovery is often neglected for heat wheels but measurements prove that this should not be done. The developed moisture recovery model is coupled with a moisture generation and ventilation simulation with moisture balance equations. The effects of using the heat wheel on indoor moisture levels are assessed for different dry and wet rooms. In general, the studied building in Oslo may experience too dry air despite the moisture recovery in the heat wheel. The moisture recovery efficiency of the heat wheel changes over time. In the simulated case, the humidity in the bedroom and living room is higher during occupancy and takes longer to reduce the higher values. The effect of moisture recovery on indoor moisture levels, often neglected in simulations, is relatively limited for the best-case scenario of moisture generation schemes in the different rooms of the studied single-family house building. Bear in mind that the absolute humidity levels of outdoor air in cold climates are low, but this effect could be more decisive for warmer climates. Also, there are only three occupants for a house of 100 $m^{2,}$ and the building is very well ventilated in this case. This article's conclusions should not be extended to other buildings with different occupancy densities, other climates, or other activity-related moisture production.

CRediT authorship contribution statement

Peng Liu: Writing – original draft, Validation, Methodology, Formal analysis, Data curation, Conceptualization. **Maria Justo Alonso:** Writing – review & editing. **Hans Martin Mathisen:** Writing – review & editing, Project administration. **Anneli Halfvardsson:** Writing – review & editing.

Declaration of competing interest

The authors declare that they have no known competing financial interests or personal relationships that could have appeared to influence the work reported in this paper.

Acknowledgement

This research was funded by the Research Council of Norway (NFR) and Flexit AS through the EnergiBolig project (NFR grant number:

256474). The authors would like to acknowledge Lars Wessman and the laboratory in Flexit for the experimental tests.

References

[1] Byggteknisk forskrift (TEK17) - direktoratet for byggkvalitet [Online]. Available: https://dibk.no/byggereglene/byggteknisk-forskrift-tek17/. (Accessed 5 December 2018).

[2] P. Wolkoff, Indoor air humidity, air quality, and health - an overview, Int. J. Hyg Environ. Health 221 (3) (01-Apr-2018) 376–390. Elsevier GmbH.

[3] K.M. Smith, S. Svendsen, The effect of a rotary heat exchanger in room-based ventilation on indoor humidity in existing apartments in temperate climates, Energy Build 116 (2016) 349–361.

[4] M. J. Alonso, H. M. Mathisen, V. Novakovic, C. J. Simonson, and L. Georges, "Review of Air-To-Air Heat/Energy Exchangers for Use in NZEBs in the Nordic Countries".

[5] P. Liu, M. Justo Alonso, H.M. Mathisen, C. Simonson, Energy transfer and energy saving potentials of air-to-air membrane energy exchanger for ventilation in cold climates, Energy Build 135 (2017).

[6] M. Justo Alonso, H.M. Mathisen, S. Aarnes, P. Liu, Performance of a lab-scale membrane-based energy exchanger, Appl. Therm. Eng. 111 (2017).

[7] P. Liu, M. Justo Alonso, H.M. Mathisen, C. Simonson, Performance of a quasi-counter-flow air-to-air membrane energy exchanger in cold climates, Energy Build 119 (2016).

[8] P. Liu, et al., A theoretical model to predict frosting limits in cross-flow air-to-air flat plate heat/energy exchangers, Energy Build 110 (Nov. 2015) 404–414.

[9] P. Liu, M.J. Alonso, M. Rafati Nasr, H.M. Mathisen, C.J. Simonson, Frosting limits for counter-flow membrane energy exchanger (MEE) in cold climates, in: 13th International Conference on Indoor Air Quality and Climate,Hong Kong, 2014.

[10] P. Liu, H.M. Mathisen, M. Justo Alonso, C. Simonson, A frosting limit model of air-to-air quasi-counter-flow membrane energy exchanger for use in cold climates, Appl. Therm. Eng. 111 (2017).

[11] C.J. Simonson, R.W. Besant, Heat and moisture transfer in desiccant coated rotary energy exchangers : Part I . Numerical model heat and moisture transfer in desiccant coated rotary energy exchangers : Part I . Numerical model, HVAC R Res. 3 (4) (1997) 325–350.

[12] C.J. Simonson, R.W. Besant, Heat and moisture transfer in energy wheels during sorption, condensation, and frosting conditions, J. Heat Tran. 120 (3) (Aug. 1998) 699–708.

[13] L.A. Sphaier, W.M. Worek, Comparisons between 2-D and 1-D formulations of heat and mass transfer in rotary regenerators, Numer. Heat Tran. Part B Fundam. 49 (3) (Sep. 2006) 223–237.

[14] R.W.B.C.J. Simonson, Energy wheel effectiveness: part 2-correlations, Journal, Int. Transf. Mass Eng. Mech. Drive, Campus (1999) 1060–1074.

[15] W. Ruan, M. Qu, W.T. Horton, Modeling analysis of an enthalpy recovery wheel with purge air, Int. J. Heat Mass Tran. 55 (17–18) (Aug. 2012) 4665–4672.

[16] I.L. Maclaine-Cross, P.J. Banks, Coupled heat and mass transfer in regenerators-prediction using an analogy with heat transfer, Int. J. Heat Mass Tran. 15 (6) (1972) 1225–1242.

[17] P.J. Banks, Coupled quilibrium heat and single adsorbate transfer in fluid flow through a porous medium-I Characteristic potential and specific capacity ratios, Chem. Eng. Sci. 27 (5) (1972) 1143–1155.

[18] D.J. Close, P.J. Banks, Coupled equilibrium heat and single adsorbate transfer in fluid flow through a porous medium - II Predictions for a silica-gel air-drier using characteristic charts, Chem. Eng. Sci. 27 (5) (1972) 1157–1169.

[19] E. Van Den Bulck, J.W. Mitchell, S.A. Klein, Design theory for rotary heat and mass exchangers-II. Effective n ess-number-of-transferunits method for rotary heat and mass exchangers, Int. J. Heat Mass Tran. 28 (8) (1985) 1587–1595.

[20] W. Zheng, W.M. Worek, Numerical simulation of combined heat and mass transfer processes in a rotary dehumidifier, Numer. Heat Tran. 23 (2) (1993) 211–232.

[22] R.K. Shah, D.P. Sekulic, Fundamentals of Heat Exchanger Design, John Wiley & Sons, 2003.

[23] J. Frauhammer, H. Klein, G. Eigenberger, U. Nowak, Solving moving boundary problems with an adaptive moving grid method: rotary heat exchangers with condensation and evaporation, Chem. Eng. Sci. 53 (19) (Oct. 1998) 3393–3411.

[24] C.E.L. Nóbrega, N.C.L. Brum, Modeling and simulation of heat and enthalpy recovery wheels, Energy 34 (12) (2009) 2063–2068.

[25] A.S. Al-Ghamdi, ANALYSIS OF AIR-TO-AIR ROTARY ENERGY WHEELS, PhD thesis, 2006.

[26] M.M. Derby, et al., Update of the scientific evidence for specifying lower limit relative humidity levels for comfort, health, and indoor environmental quality in occupied spaces (RP-1630), Sci. Technol. Built Environ. 23 (1) (Jan. 2017) 30–45.

[27] P. Wolkoff, The mystery of dry indoor air - an overview, Environ. Int. (01-Dec-2018) 1058–1065. Elsevier Ltd.

[28] P.J. Annila, J. Lahdensivu, J. Suonketo, M. Pentti, J. Vinha, Need to repair moisture- and mould damage in different structures in Finnish public buildings, J. Build. Eng. 16 (Mar. 2018) 72–78.

[29] P.J. Annila, M. Hellemaa, T.A. Pakkala, J. Lahdensivu, J. Suonketo, M. Pentti, Extent of moisture and mould damage in structures of public buildings, Case Stud. Constr. Mater. 6 (Jun. 2017) 103–108.

[30] FHI, Temperatur, fukt og trekk er viktig for kroppens varmebalanse - FHI [Online]. Available: https://www.fhi.no/ml/miljo/inneklima/artikler-inneklima-og-helseplager/temperatur-fukt-og-trekk-er-viktig-/. (Accessed 1 January 2021).

[31] Technical concepts to avoid low relative humidity – FME ZEN [Online]. Available: https://fmezen.no/technical-concepts-to-avoid-low-relative-humidity/. (Accessed 5 October 2020).

[32] S. Geving, J. Holme, Mean and diurnal indoor air humidity loads in residential buildings, J. Build. Phys. 35 (4) (Apr. 2012) 392–421.

[33] J. Vinha, M. Salminen, K. Salminen, T. Kalamees, J. Kurnitski, M. Kiviste, Internal moisture excess of residential buildings in Finland, J. Build. Phys. 42 (3) (Nov. 2018) 239–258.

[34] T. Kalamees, J. Vinha, J. Kurnitski, Indoor humidity loads and moisture production in lightweight timber-frame detached houses, J. Build. Phys. 29 (3) (Jan. 2006) 219–246.

[35] V. Leivo, M. Kiviste, A. Aaltonen, T. Prasauskas, D. Martuzevicius, U. Haverinen-Shaughnessy, Analysis of hygrothermal parameters in Finnish and Lithuanian multi-family buildings before and after energy retrofits, Orig. Artic. J. Build. Phys. 42 (4) (2019) 441–457.

[36] S. Ilomets, T. Kalamees, J. Vinha, Indoor hygrothermal loads for the deterministic and stochastic design of the building envelope for dwellings in cold climates, J. Build. Phys. 41 (6) (May 2018) 547–577.

[37] BS EN 308:1997, Heat Exchangers. Test Procedures for Establishing the Performance of Air to Air and Flue Gases Heat Recovery Devices, 1997.

[38] C.J. Simonson, HEAT AND MOISTURE TRANSFER IN ENERGY WHEELS, 1998.

[39] C.E. Rasmussen, C.K.I. Williams, Gaussian processes for machine learning [Online]. Available: https://mitpress.mit.edu/books/gaussian-processes-machine-learning. (Accessed 2 January 2021).

[40] F.W.H. Yik, P.S.K. Sat, J.L. Niu, Moisture generation through Chinese household activities, Indoor Built Environ 13 (2) (Apr. 2004) 115–131.